2012-01-01

Electrical Characterization Of Microcrystalline LiFePO4 For Application In Lithium Ion Batteries

Sukhdeep Amarjeet Labana
University of Texas at El Paso, salabana@miners.utep.edu

ELECTRICAL CHARACTERIZATION OF MICROCRYSTALLINE $LiFePO_4$ FOR APPLICATION IN LITHIUM ION BATTERIES

SUKHDEEP A. LABANA

Department of Electrical and Computer Engineering

APPROVED:

C. V Ramana, Ph.D., Chair

Joseph H. Pierlussi, Ph.D.,

Thompson Sarkodie-Gyan, Ph.D.,

Yirong Lin, Ph.D.

Benjamin C. Flores, Ph.D.
Interim Dean of the Graduate School

DEDICATION

To my parents and siblings

ELECTRICAL CHARACTERIZATION OF MICROCRYSTALLINE $LiFePO_4$ FOR APPLICATION IN LITHIUM ION BATTERIES

by

SUKHDEEP A. LABANA, B.S.E.E

THESIS

Presented to the Faculty of the Graduate School of

The University of Texas at El Paso

in Partial Fulfillment

of the Requirements

for the Degree of

MASTER OF SCIENCE

Department of Electrical and Computer Engineering

THE UNIVERSITY OF TEXAS AT EL PASO

August 2012

ACKNOWLEDGEMENTS

This dissertation would not have been possible without the guidance and the help of several individuals who in one way or another contributed and extended their valuable assistance in the preparation and completion of this study.

I would like to express my deepest gratitude to my advisor, Dr. C V Ramana, for his excellent guidance, caring, patience, and providing me with an excellent atmosphere.

Dr. Pierluissi**,** Department Chair for Electrical & Computer Engineering, for the moral support and kind concern regarding my academic requirements.

The Administrative Secretary of Electrical Engineering, Linda Romero for being accommodating to my queries and student assistant for all the help.

I would also like to thank my parents, and siblings Bhupinder, Mandeep, Kabir and Tohfa. They were always supporting me and encouraging me with their best wishes.

Finally, I would like to thank my fiancé, Robby Ravinder Singh. He was always there cheering me up and always willing to help and give his best suggestions.

TABLE OF CONTENTS

LIST OF TABLES

LIST OF FIGURES

CHAPTER 1: INTRODUCTION

When considering electrical storage devices, lithium-ion batteries represent the cutting edge of technology in providing superior performance with widespread and efficient applications in various different platforms. The lithium-ion battery generally falls within the family of rechargeable batteries governed by a mechanism where lithium ions move from a negative electrode to a positive electrode during the course of usage or discharge. During a state of charging, on the other hand, lithium ions move from a positive electrode to a negative electrode.

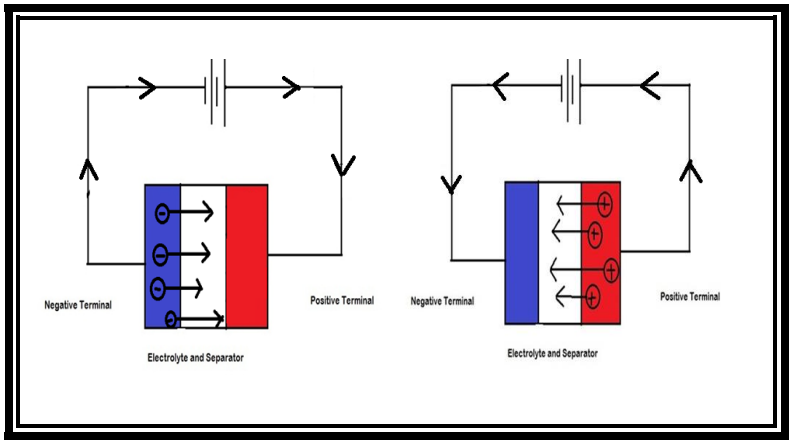

Figure 1: Schematic Diagram of a Lithium Ion Battery

The schematic diagram of a battery and its operating principle is shown in Fig. 1. There are three primary components which include the negative electrode, positive electrode, and the electrolyte. The negative electrode or anode of the lithium-ion cell is comprised of carbon. The positive electrode or cathode is generally constituted by a metal oxide. Finally, the electrolyte is a lithium salt in an organic solvent.[1]

When considering the cost of lithium-ion batteries based on its structural properties and constituents they are often more expensive when compared to alternatives such as nickel cadmium (NiCd) and are generally more fragile. Despite these potential drawbacks, lithium-ion batteries operate over a wide range of temperatures and enjoy higher energy densities.

Lithium-ion batteries with a $LiCoO_2$ cathode and carbon anode were introduced by SONY in early 1990s[2] At the time of its introduction, the lithium-ion battery offered advantages in high-energy density, increased power, and long service life making them appropriate for several applications in the realm of consumer electronics including mobile phones, laptops and power tools. The material comprising the cathode in lithium-ion batteries is known as lithium cobaltite which falls under the $LiCoO_2$ series. This family of compounds consists of a condensed network of oxygen and lithium atoms along with a transition metal (M) which occupies ordered and alternating layers between the planes. The compounds that fall within the $LiCoO_2$ series, such as lithium cobaltite, represent a lamellar-type rock-salt structure.

Despite the common use of cobaltite in the construction of cathodes in lithium-ion batteries, the inclusion of other viable elements ought to be considered. In terms of prevalence, iron (Fe) is a rather attractive option as is often used to build significantly sized batteries in providing power in appropriate applications such as electric vehicles. In terms of abundance, iron is exceeded only by aluminum, silicon, and oxygen within the Earth's crust. As a testament to its practicality, the earliest record of iron used by man dates back to at least 2000 BC[3]. Unfortunately, despite its variety of uses, iron and its derivatives have been ineffective as constituents for electrode material in lithium-ion batteries. When considering Fermi energy in regards to a lithium anode, iron-based oxides containing O^{2-} as an anion yields Fe^{4+}/ Fe^{3+} resulting in redox energy that falls too low to be feasible. When considering the Fe^{3+}/ Fe^{2+}couple, the redox energy falls to close to thresholds regarding Fermi energy. The issue of extremes when considering iron for lithium-ion batteries makes its use problematic. The thought process regarding the use of iron in lithium-ion batteries based on different cathode materials informs an overall discussion of various lithium-ion strategies. There are three fundamental strategies in regards to cathode materials and include lithium cobalt oxide, lithium manganese oxide, and lithium iron phosphate types. Evaluating each strategy is important in weighing potential pros and cons to determine the most expedient proposal. The strength of lithium cobalt oxide lies in its high energy density but is hampered by safety concerns. An advantage of lithium manganese oxide has been its use in high-demand applications and has exhibited increased effectiveness over previous lithium strategies. One of the disadvantages of lithium manganese oxide has been its poor performance in high temperature conditions. Finally, when evaluating lithium iron phosphate, it has been found to have the best safety characteristics, long cycle life lasting up to 2000 cycles, and considerable accessibility. In addition, lithium iron phosphate has been found to be capable in meeting the demands of high discharge requirements in a variety of applications such as military use, electrical vehicles, power tools, mobile devices, and solar energy systems.

Lithium iron phosphate for electrochemical energy storage device applications was first proposed and demonstrated by John Goodenough's research group at the University of Texas in 1996[4]. The discovery of $LiFePO_4$ was mainly due to its applicability as a cathode material for rechargeable lithium batteries. The work by Goodenough's research group opened up the door to a new lithium iron phosphate battery with cells large enough for use in greater-demand applications, such as hybrid cars. Furthermore, the research has expanded the field of battery consumption with claims of potentially being "the largest cells of their kind in the world."[5]

In addition to the advantages of larger-scale batteries with lithium iron phosphate, another advantage lies in the assimilation of phosphates as the cathode material resulting in greater, positive safety characteristics. Phosphates are extremely stable in short circuit conditions and are capable of withstanding high temperatures without decomposing. Building upon the use of safer phosphates, most lithium-ion batteries also use organic solvents as the electrolyte. The most commonly used organic solvent being $LiPF_6$ (lithium hexafluorophosphate) which contributes to overall lower electrical resistance[6] typically mixed with carbonates. Because of its low cost, characteristics of non-toxicity, high levels of abundance, excellent thermal stability, safety characteristics, good electrochemical performance, and high specific capacity (170mA·h/g) the use of iron has gained considerable market acceptance[7]. The key barrier to commercialization was its intrinsically low electrical conductivity.

The electrical conductivity problem has been the focus of attention of many researchers. Reducing the particle size and effectively coating the $LiFePO_4$ particles with conductive materials such as carbon has been considered to improve the electrical conductivity of the material. In addition, doping with metal ions and related approaches were also seems to be helpful[8]. The approaches involved cations consisting of materials such as aluminum, niobium, and zirconium. Approaches based on synthetic route modifications were also considered in the literature. It was shown that the conductivity improvement was due to the presence of nanoscopic carbon originating from organic precursors during synthesis[9]. Products using the carbonized and doped nanophosphate materials are now in high volume mass production by A123Systems and other companies. Investigating the viability of the lithium iron phosphate battery further, it has been found to shares many advantages and disadvantages with other lithium ion battery chemistries. Some of the drawbacks using LFP batteries include rapid charging of the lithium-ion battery. Such a mechanism may result in the lithium-iron phosphate shortening the life span or partilar batteries as compared to traditional trickle charging. Reserves of lithium may also be a concern as estimates in the year 2015 are projected at 30,000 tons[10]. Another drawback in the use of lithium-iron phosphate is its specific energy (energy/volume) where a new LPF battery is somewhat lower as compared to a new battery. Battery manufactures across the world are currently working to find ways to maximize the energy storage performance while concurrently reducing the considerable size and weight associated with using lithium iron phosphate[11]. Another cause of concern involves scenarios where LFPs are “deep cycled” or discharged below a threshold of 33%. If this occurs too early in overall battery life, lithium iron phosphate based batteries have been found to fail prematurely. A “break-in period” or series of 20 cycles in order to acclimate the battery is currently recommended by some distributors.

Ultimately, the disadvantage of lithium iron phosphate cells as compared to lithium cobaltite cells in lithium-ion batteries lies in lower average voltage and energy density levels. Yet, this disadvantage of lithium iron phosphate is counterbalanced over time by a slower rate of capacity loss. When compared with other lithium-ion polymer batteries or standard lithium-ion battery chemistries such as $LiCoO_2$ (cobalt) or $LiMn_2O_4$ (manganese spinel), lithium iron phosphate exhibits an overall greater calendar life[12]. Typically after a full year of use, a $LiFePO_4$ cell and $LiCoO_2$ cell will have approximately the same energy density around average levels. The difference lies in going beyond a full-year of use where lithium iron phosphate cells is likely to have higher energy density levels.

After considering these preliminary perspectives in the feasibility of lithium iron phosphate cells for potential use in lithium ion battery, it is also important to recognize possibilities that go beyond viability and venture into the realm of potential advantages. Further analysis of structural and morphological properties of lithium iron phosphate along with other applications is necessary to make such a case. Building upon the strength of past research findings through experimental approaches, greater understanding of lithium iron phosphate could lead to greater efficiency and effectiveness in meeting modern-day demands and potentially opening the door for future directions.

CHAPTER 2: MOTIVATION AND SIGNIFICANCE

2.1 Cathode Material

Cathode materials are typically oxides of transition metals, which can undergo oxidation to higher valences when lithium is removed [13, 14]. Large compositional changes results to phase changes during the time of charge neutrality. Therefore, the stable crystal structures must be used over wide range of composition. During charging most of the lithium is removed from the cathode. However, during discharging the electrons from anode reduces the transition metal ions in the cathode when lithium is inserted into the cathode material. $LiMPO_4$ class of cathode materials with the olivine structure (Pnma), in which phosphorous occupies tetrahedral sites, the transition metal (M) occupies octahedral sites and lithium forms one-dimensional chains along the [0 1 0] direction [15]. The phosphate most commonly used for the cathode is $LiFePO_4$, which delithiates to $FePO_4$ as the Fe^{+2} is oxidized to Fe^{+3} [16]. Some iron ions occupy lithium sites, which results in the formation of lithium ion-vacancies to maintain charge neutrality [17-19]. There is a miscibility gap between $FePO_4$ and $LiFePO_4$[20], so the delithiation occurs by growth of a two-phase front rather than a continuous change in lithium content [21-26]. The formation of a two-phase mixture establishes a fixed activity, which results in a relative flat discharge profile (i.e. the voltage remains relatively constant during discharge) [27]. Electronic conduction in $LiFePO_4$ occurs by small polaron hopping [28] and is relatively low ($10^{-9}cm^{-1}$) for pure $LiFePO_4$[29]. Conductivity can be improved by heat treating to increase the hole conductivity phase [30] is generally needed for satisfactory performance [31].

A critical factor for its electrochemical performance is represented by the low electronic conductivity [32]. Lithium ion requires simultaneous passage of electrons between the two sites. The ionic diffusivity is limited by the low electronic diffusivity if ionic conductivity is higher than the electronic conductivity. Lithium ion insertion in lithium iron phosphate results in the co-existence of two phase formation (i.e. non-continuous). However, Mc. Kinnon and Hearing found it is not possible to distinguish between two diffusion models based on continuous or non-continuous process of lithium ion removal or uptake [33].

The process of diffusion is still in discussion. Based on the theoretical expression Manro Pasquali and Pier Paolo Prosini described the Fitting of the voltage-Li ion insertion curve of $LiFePO_4$ in a solid medium. Also the different discharge stages were theoretically obtained from the polarization curve resulting in good agreement at high discharge rate.

$LiFePO_4$ crystallizes in the space group of the olivine structure as shown in the Figure 2. In the bc plane the FeO_6 octahedra sharing forms the layers which are linked together by PO_4 tetrahedral unit. The lithium ions are located between the Fe-O layers that are blocking for the Li diffusion in the space left by the PO_4 units. Yet the b and c directions are not equivalent, and the energy barrier that the Li has to overcome to move from one unit cell to the next one is 0.55 eV along the b-direction, compared with 2.89 eV along the c-direction [34]. In practice, the Li-ions will move along the path that requires a minimum energy, so that they will "slalom" in the b-direction[35]. The motion is then one-dimensional. This information, however, is not sufficient to understand the ionic conductivity in the lithiation/delithiation process, because the motions of neighboring Li ions are correlated. This correlation is best shown by the fact that the solid solution $LixFePO_4$ does not exist under "normal" conditions in particles that are large enough so that size effect are negligible [36].

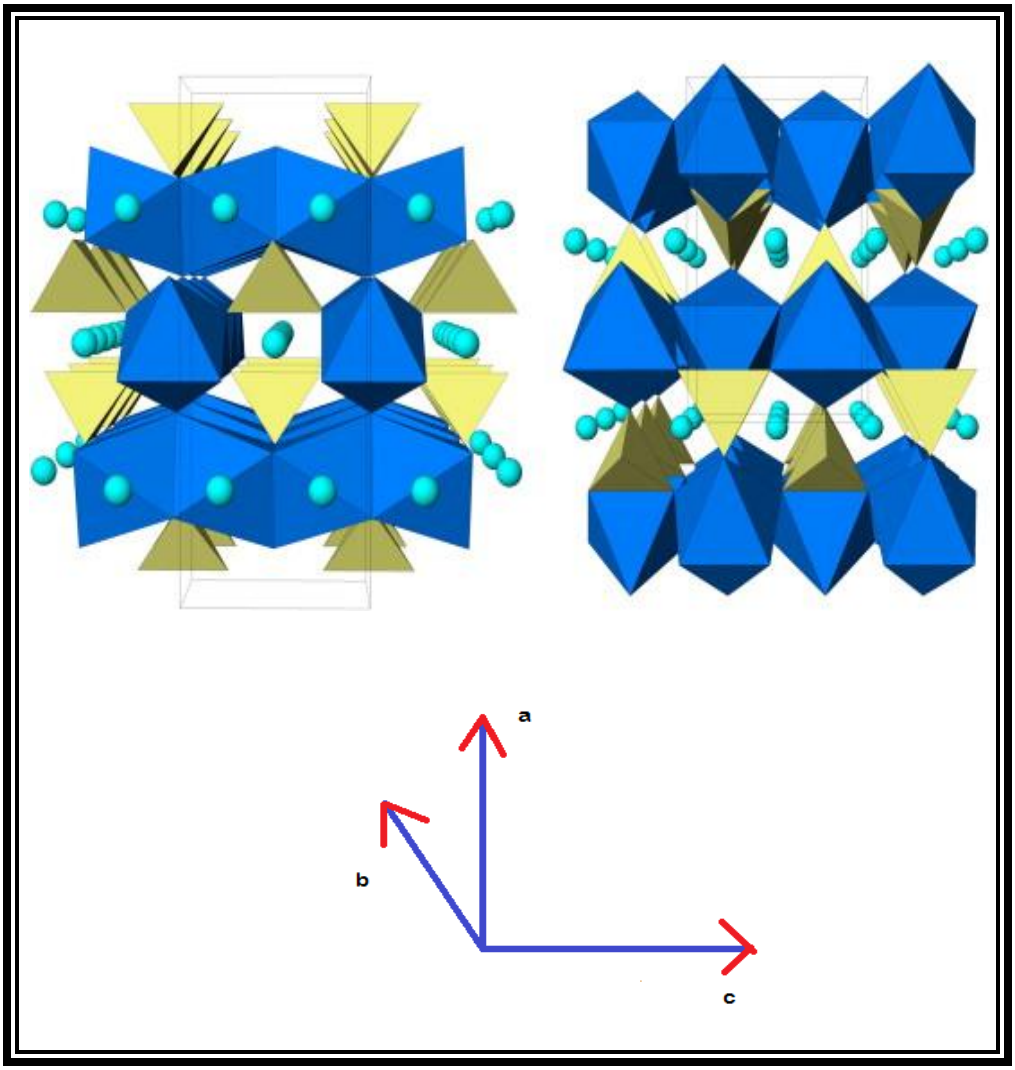

Figure 2: Tunnel structures of (left) lipscombite, $Fe_{1.33}PO_4OH$, and (right) olivine, $LiFePO_4$, showing the FeO_6 octahedra, PO_4 tetrahedra, and the one-dimensional tunnels in which the lithium ions reside [37]

2.2 Cathode Performance and Composite Cathodes

The operating voltages and capacities of $LiFePO_4$[38,39-48] and $LiCoO_2$[49-53] with a charging voltage of 4.2V and discharging current of 1C shows the operating voltage for $LiCoO_2$ is higher than for $LiFePO_4$. The narrow voltage range of $LiFePO_4$is a due to the formation of a two-phase mixture.

The combination of two a composite electrode can be used to improve performance [54]. For example the addition of $LiFePO_4$ to other electrode, including $LiCoO_2$[55,56], Li $(Li_{0.17}\ Mn_{0.58}\ Ni_{0.25}\ )O_2$[56] and $Li(Ni_{0.25}\ Mn_{0.3}\ Co_{0.2}\ )O_2$ [57] improves capacity retention during cycling and performance at high discharge currents. Similarly, a phosphate surface treatment can improve capacity [58] or performance after cycling[59] of oxide electrodes.

2.3 Effect of Doping

The performance of cathode materials can be improved by doping, but due to interrelations between doping and microstructure and morphology, the doping effects can be complicated. Carbon is commonly added to cathodes to more effectively utilize the active cathode materials, especially at high discharge rates. Carbon additions improve the performance of $LiFePO_4$[60,61-63] which has a relatively low electrical conductivity. The effectiveness of carbon additions depends on the amount and type of carbon used. A thin carbon layer can provide a path for electrons without blocking access for Li ions [64,65] . Graphite carbon generally provides higher conductivity and thus higher rates capacities at larger discharge rates, so carbons with large $sp_{2/}\ sp_3$ ratios are generally preferred [66-69]. The particular shape is also important as nano-scale fibers [70-76] and high surface area forms of carbon, such as acetylene black [77,78] have been shown to be effective in improving cathode performance.

Improvements in rate capability have been achieved and reported in many research papers [79-83], including mixing in fine particles[84], particle size control [85], doping with a conductive metal ion[86] and carbon coating [87]. Different kinds of carbon coating methods are used to increase the electronic conductivity of $LiFePO_4$. These methods contain the post synthesis [88] by co grinding and co firing with organic or polymeric addictives [89,90] to produce coated particles. With larger amounts of carbon and decrease volumetric energy density the rate capability increases. On the other hand, the structure and amount of carbon content will strongly influence the electronic conductivity of $LiFePO_4$/C composite materials. Therefore, to avoid decreasing the volumetric energy density, the amount of carbon should be kept low and more efficient. The $LiFePO_4$/C composite material which have a continuous and dispersive nano-carbon network show high electronic conductivity and rate capability [91]. The morphology studies of $LiFePO_4$/C composite materials were conducted using a field emission scanning electrons microscope (FE-SEM, JEOL, and JSM-6340F). The transmission electron microscope bright image and EELS mapping are used to find the microstructure and nano-carbon channels of pure $LiFePO_4$and composite $LiFePO_4$[91]. From the TEM bright field image and EELS mapping, the $LiFePO_4$/C powder shows continuous, dispersive nano-carbon network.

2.4 Scope and Significance of the Present Work

Understanding the electronic behavior, electrochemical reactions and charge transport in the $LiFePO_4$ cathode material is of paramount importance. The ability to tailor the properties so as to optimize battery performance requires a detailed fundamental understanding and manipulation of electronic properties of $LiFePO_4$. The present work was, therefore, performed on $LiFePO_4$ microcrystalline material to understand the electrical and dielectric properties and various conduction mechanisms at various temperature ranges. Impedance spectroscopy (IS), which is a major part of this work, is an important analytical method to determine the independent transport parameters such as electronic/ionic conductivities, diffusion coefficients, and rate constants for electrochemical reactions in

$LiFePO_4$. Impedance spectroscopy requires knowledge about different conduction processes and physical origin of all processes contribute to the total impedance. In addition, impedance analysis is the best tool to determine the contributions of grain boundaries and bulk of the grains to the electronic conduction. The individual contributions can be conveniently separated by using appropriate analytical and equivalent circuit models. Specific capacity of $LiFePO_4$ critically depends on the factors such as electronic conductivity, diffusion of Li^+ ion in the olivine structure, preparation method and the powder structure. Microstructure, chemical composition and operating temperature are the important factors, which influence the charge, discharge capacity and rate performance of $LiFePO_4$. The obvious relevance of the work is, therefore, to examine the frequency and temperature dependent AC and DC electrical properties of $LiFePO_4$ material. Also, to the best of our knowledge, there are no existing reports on the detailed studies on the temperature and frequency depended dielectric, impedance and AC conductivity of microcrystalline $LiFePO_4$ and the correlation between these electronic properties is missing. Therefore, such an investigation using combined AC and DC electrical conductivity measurements is expected to contribute significantly to our current understanding of the conduction process and associated mechanisms in $LiFePO_4$. The results obtained are presented and the effect of temperature and frequency on conductivity, dielectric properties and the conduction mechanisms of $LiFePO_4$ are discussed in this thesis.

CHAPTER 3: EXPERIMENTAL DETAILS

3.1 Synthesis

$LiFePO_4$ was prepared by the solid state reaction method. The starting materials were Li_2CO_3, $FeC_2O_4.2H_2O$ (99.99%) and $NH_4H_2PO_4$ (99.99%). These materials were ground in a mortor pestle for one hour, have been first ball milled during 1 hr 30 min. and then heat treated in a tube furnace under argon flow for 8 hr. at 800 ^oC. For the electrical measurements the powders were made into pellets which were then sintered at 800 ^oC in air.

3.2 Scanning Electron Microscopy (SEM)

3.2.1 PRINCIPLE OF OPERATION

When electron beam falls on the sample the weakly bond electron from sample surface get ejected and produce the secondary electrons. Secondary electrons are of low energy it can be easily detected by the detector to produce the SEM image of the sample surface. Low energy of secondary electron it get influenced by the electromagnetic field. To avoid the charge built on sample surface is proper conducted using Copper tapes. The Hitachi 4800 SEM employed in this work in shown in Fig. 3.

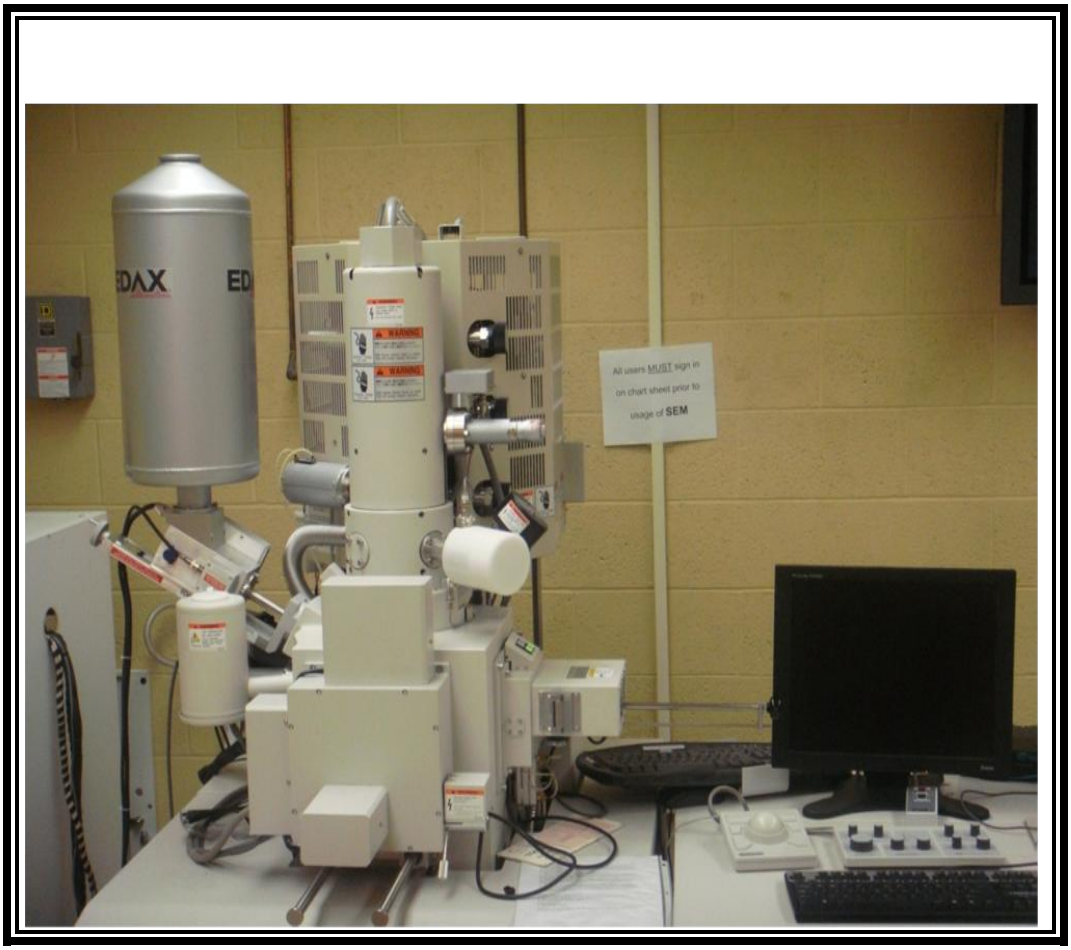

Figure 3: Hitachi S-4800 Scanning Electron Microscope

3.2.2 OPERATION/ WORKING

In SEM electron thermionically emitted from tungsten cathode filament are drawn to an anode (Fig. 4). Electron beam energy ranging from 0.5 KeV to 40 KeV canbe employed. Two condenser lenses in vacuum chamber are used to focus in very small surface area of 1 nm to 5 nm in diameter. High energy electron beam hits the sample; the high energy electron beam loses it energy by random scattering and absorption. The low energy electron is called as secondary electrons. Due to their low

energy, these electrons originate within a few nanometers from the sample surface. The secondary electron is detected by the detector to shows the SEM image.

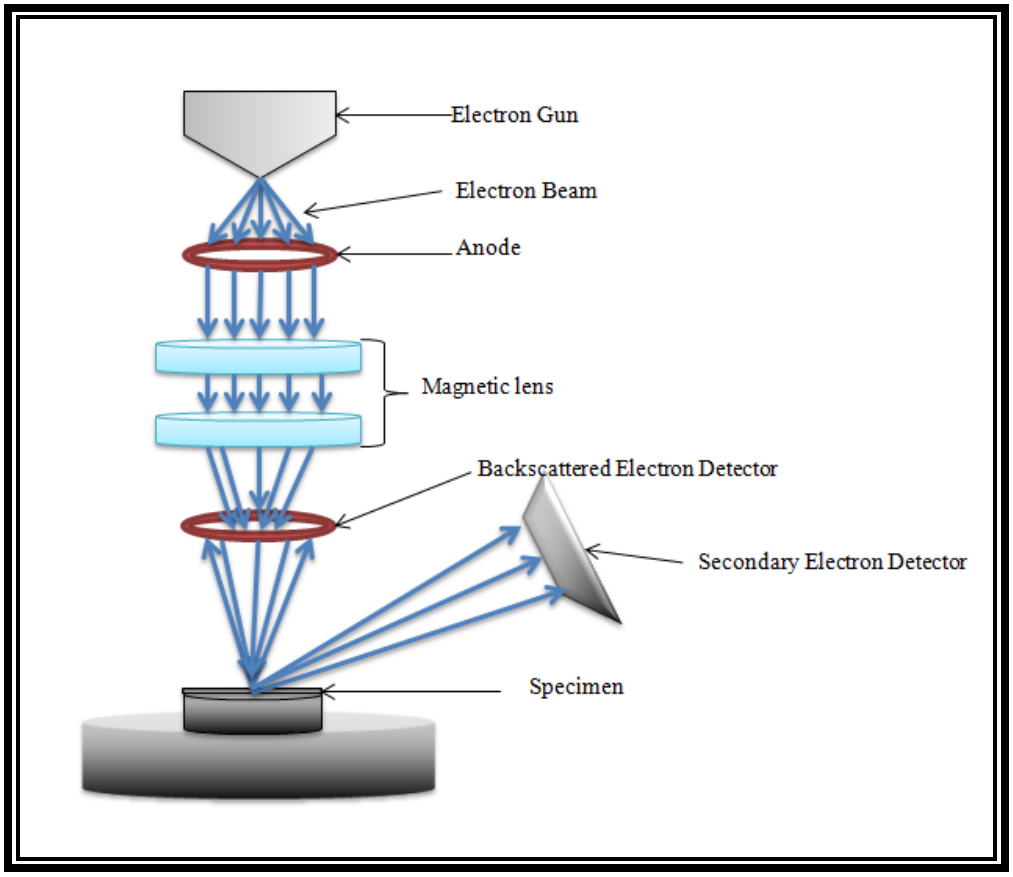

Figure 4: Working principle of SEM

3.3 Crystal Structure

A Bruker D8 Advance X-Ray diffractometer (XRD) (Fig. 5) has been used for the structural characterization. The crystal structure, preferred crystallographic information (if any), crystallite size, and the phases were determined from XRD patterns. In XRD technique the material is irradiated by the parallel beam of X-ray, which gets diffracted from the atomic lattice structure of the film which act as a three dimensional lattice causing the x-ray to diffracted at specific angle.

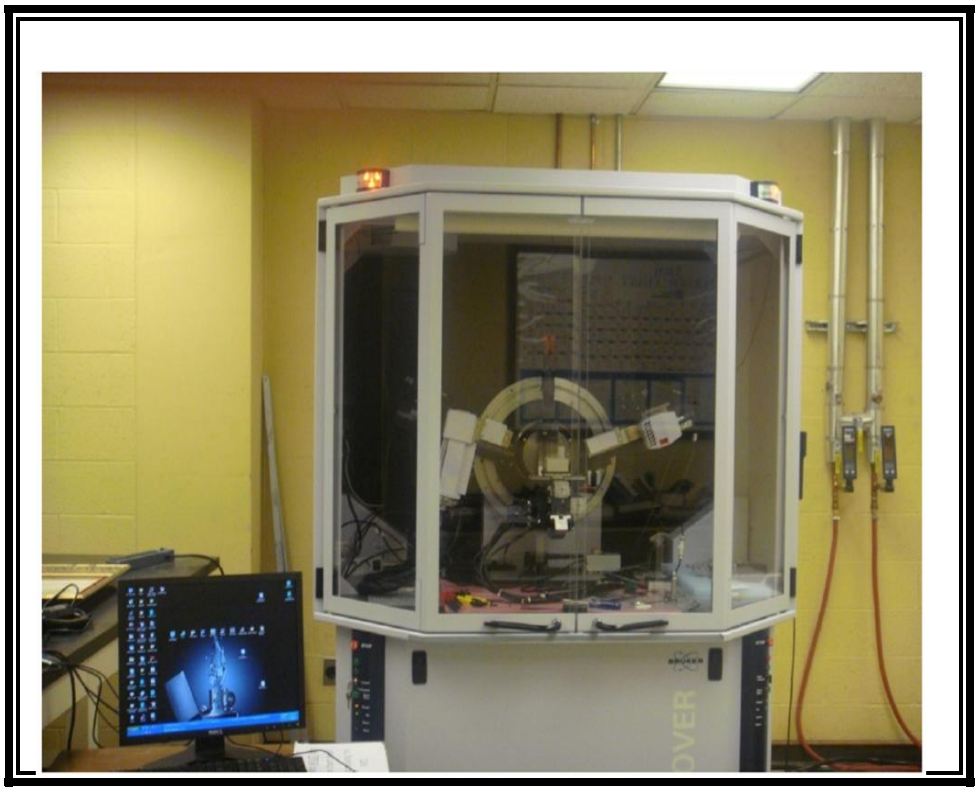

Figure 5: Bruker D8 Advance X-ray diffractometer

The diffracted x-rays beam provides several information about the film crystallography and inter-planar atomic distance 'd' between the two planes of the film. Angle θ are used to calculate the inter-planar atomic distance of the film using Bragg's law:

$$n\lambda = 2d \sin \theta \qquad (1)$$

where λ = wave length of X-ray, d = inter planar distance and θ = Bragg's angle.

All the measurement was made ex-situ as a function of growth temperature. XRD pattern were recorded using CuKα radiation (λ=1.54056Å) at room temperature.

3.4 Electrical Conductivity

For conductivity measurement, fine powder of $LiFePO_4$ was pelletized between thin layers of ultra fine graphite powder. The electrical measurements were made in a home built apparatus. The sintered $LiFePO_4$ pellet was mounted between two spring-loaded electrodes in an evacuated conductivity setup (vacuum of 10^{-2} Torr). The ac impedance data, $|Z|$ and phase angle were recorded using a HP4192A impedance analyzer over the temperature range of 300–473 K.

CHAPTER 4: RESULTS AND DISCUSSION

4.1 Structure

The X-ray diffraction patterns obtained for $LiFePO_4$ are presented in Fig. 6. The calculated pattern after the Rietveld refinement carried out using the GSAS program[92] is also shown in Fig. 6. The wrp (weighted refined parameter) and the χ^2 (goodness of the fit) values of the fitting are 0.03 and 1.00, respectively.

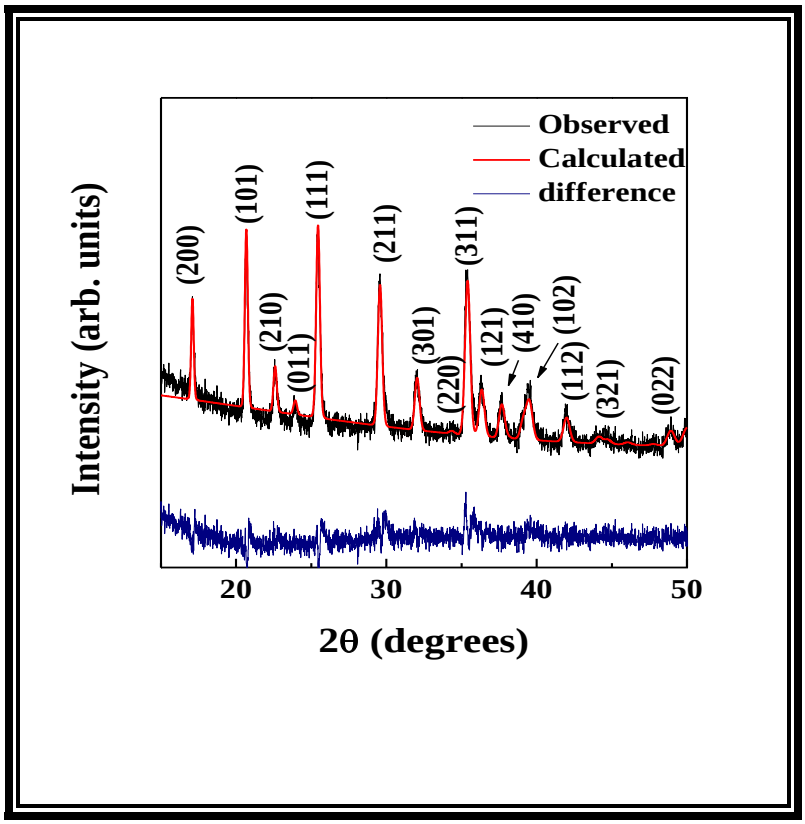

Figure 6: XRD pattern of LiFePO4

$LiFePO_4$ was found to form in the Pnma space group with olivine-type structure without any impurity phase. The calculated values of the lattice constants are a=10.4093 (±0.002 Å) Å, b=6.0500 (±0.002 Å) Å and c=4.7315 (±0.002 Å) Å, which are in close agreement with that of the reported values.[93] The Li-O and Fe-O bond lengths in the LiO_6 and FeO_6 octahedra are found to be 2.18 Å and 2.22 Å, slightly larger than the reported values. The small expansion in the lattice can be viewed as a prominent Jahn-Teller distortion of the lattice coupled to the orbital moment (L) of Fe^{2+}/ Fe^{3+} ion. The refined atomic fractional coordinates are given in Table 1. The results obtained by Rietveld refinement are satisfactory, as suggested also by the reliable values of the discrepancy factors wrp (5%) and χ^2 (1.00) values.

Table 1: Refined atomic position values of $LiFePO_4$.

Atom	X (±0.002 Å)	Y (±0.002 Å)	Z (±0.002 Å)
Li	0	0	2345
Fe	0.2822	0.2500	0.9747
P	0.0948	0.2500	0.4182
O1	0.0967	0.2500	0.7427
O2	0.4571	0.2500	0.2060
O3	0.1655	0.4646	0.2847

The SEM image of $LiFePO_4$ compound is shown in Fig. 7. Uniform size and shape of the particles are clearly seen from the SEM image. Presence of Fe, P and O ions are confirmed from the EDX analysis (Fig. 7).

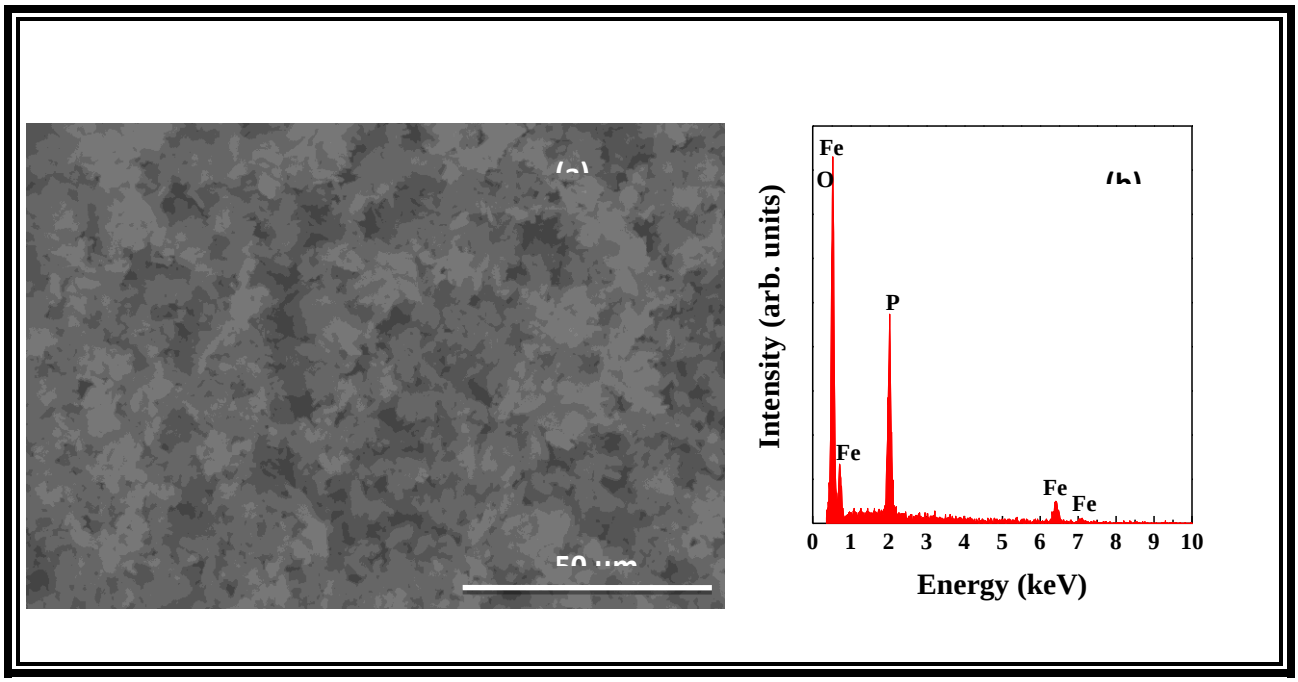

Figure 7: (a) High resolution SEM image of LiFePO4 powders. (b) EDX spectra of LiFePO4, indicating the presence of Fe, P and O elements. Li ion was not identified by the instrument.

4.2 Electrical Impedance Analysis

The impedance of $LiFePO_4$ was measured in the frequency range 10 Hz - 13 MHz (at 300 – 473 K). The frequency variation of the real part of impedance (Z') at selected temperatures for $LiFePO_4$ is shown in Fig. 8. The decrease in the value of Z' with increasing frequency indicates that the conductivity of the $LiFePO_4$ increases as the frequency increases. This can be attributed to the increase in hopping of electrons between the localized ions. Z' is seen to decrease with increasing temperature in $LiFePO_4$.

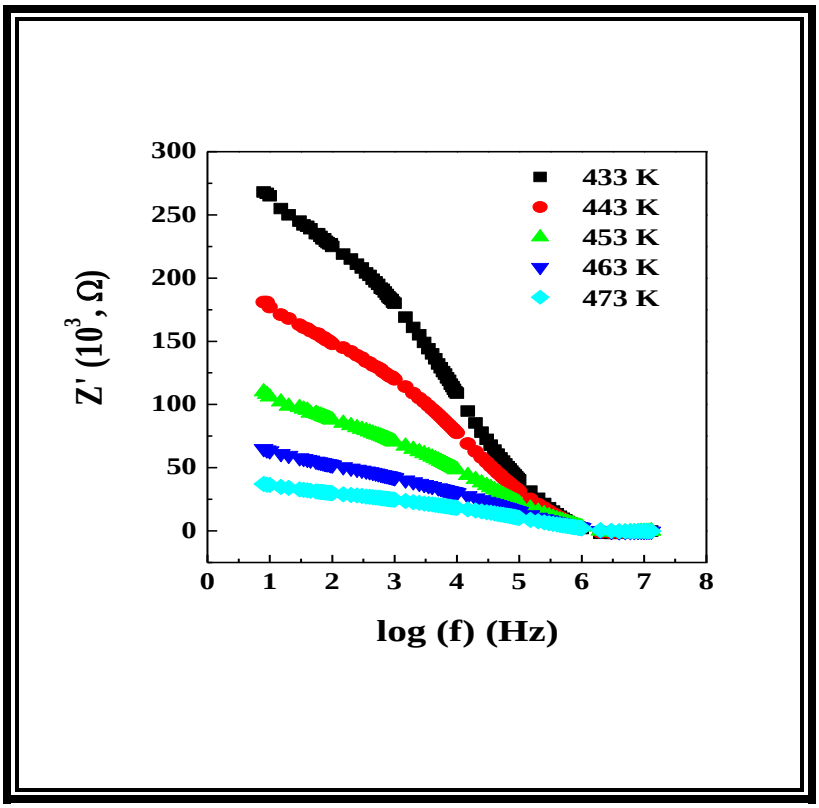

Figure 8: Frequency variation of real part of impedance (Z') of LiFePO4 at different temperatures

Impedance of a polycrystalline material can be expressed as[94-96]

$$Z = Z^{'} + jZ^{''} = R + \frac{1}{j\omega C} \qquad (2)$$

where

$$Z' = \frac{1/R}{(1/R^2) + \omega^2 C^2} \qquad (3)$$

and

$$Z^{''} = \frac{-\omega C}{1/R^2 + \omega^2 C^2} \qquad (4)$$

R, C, and ω represents resistance, capacitance and angular frequency, respectively, and j=√-1. Here in these equations, the unit for real (*Z′*) and imaginary (Z′′) parts of impedance and resistance R is ohm (Ω) and that of capacitance C is Farad (F). It has been reported[97] that, with increasing temperature, lithium ion loss occurs in $LiFePO_4$ due to the following reactions. Li reacts with oxygen (O_2) or H_2O and forms Li_2O or LiOH and stoichiometry of $LiFePO_4$ changes in small amount. Therefore, with increasing temperature electronic conductivity increases due the increase in Li loss, hence Z′ decreases.

Figure 9 shows the variation of imaginary part of impedance (Z′′) as a function of frequency at different temperatures. Z′′ is seen to decrease with increasing temperature due to the decreasing loss in the resistive part of the sample. Z′′ decreases with increasing frequency and exhibits broad Debye peaks, which is an indicative of the existence of relaxation processes in this material.[94-96] Asymmetric nature of the Debye peaks observed is a characteristic of the distribution of relaxation process and relaxation time in $LiFePO_4$. Observation of Debye relaxation peaks in the imaginary part of complex impedance at low frequencies is due to the presence of the space–charge relaxation which is associated with the charge carriers in connection with the oxygen vacancies.[94-96]

According to Koop's theory[98], space charge polarization occurs when the material contains hetero-structures or different regions (grain and grain boundaries). At low temperatures electrical conductivity in $LiFePO_4$ is mainly due to the short range hopping of electrons or polarons. Space charge polarization at low frequencies and temperatures occurs due to the following reactions. High mobility oxygen vacancies are trapped at the electrode ($LiFePO_4$ pellet) surface and they travel with faster rate when the external AC field is applied leading to the space charge effect. Debye peaks occur when the hopping frequency of electron becomes equal to the frequency of the external applied electric field. With the increasing temperature, Debye peaks are seen to move in the higher frequency side (Fig. 9).

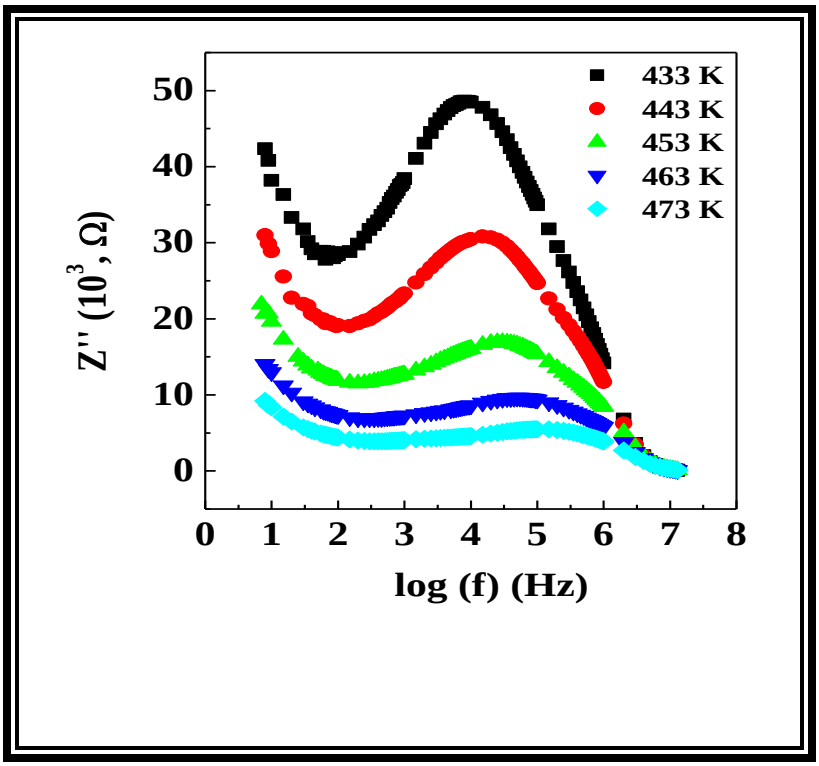

Figure 9: Frequency variation of imaginary part of impedance (Z'') of LiFePO4 at different temperatures

The shifting of these peaks to higher frequency side can be attributed to the increased electron hopping rate in $LiFePO_4$.The plots of the real ($Z^{'}$) *versus* imaginary ($Z^{''}$) parts of impedance (Cole-Cole plot) at various temperatures are shown in Fig. 10. Incomplete semicircle was observed at room temperature due to the high resistance values at low frequencies.

At temperatures above 330 K, single semi-circle is observed at various temperatures for $LiFePO_4$. For polycrystalline $LiFePO_4$, impedance Z can be expressed as[94-96]

$$Z = R_g + \frac{1}{j\omega C_g} \qquad (5)$$

where R_g (Ω) and C_g (F) represents the resistance and capacitance of the grain. The value of R_g was obtained from the diameter of the semi circle and C_g was calculated using the relation ωRC = 1, at maximum Z″ point in semicircle. The calculated value of R_g and C_g values at different temperature are listed in Table II. R_g value is found to decrease from 252 to 91 k Ω (±1 Ω) with increasing the temperature from 433 to 453 K. C_g value increases from 1.01 to 2.48 10^{-8} F with increasing the temperature from 433 to 453 K. Straight line on the low frequency side is due to the electrolyte–electrode polarization at the blocking electrodes. Amin and Maier[97] have reported that impedance spectra of $LiFePO_4$ at various temperatures consist two depressed semi-circles corresponds to bulk grain and grain boundary conduction. Resistance due to the grain boundary conduction is large compared to the bulk grain and the conduction is due to electronic conductivity. In the present case, single semicircle in observed at various temperatures and it is usually assumed to account for the intrinsic bulk grain contribution to R_g and C_g due to the predominant contribution from grain. The contribution from the grain boundary to the resistance and capacitance is not observed in the present case. The relaxation time τ_g (ms) at different temperatures (Table II) are calculated from the relations

$$\tau_g = \frac{1}{\omega_g} = R_g C_g \qquad (6)$$

τ_g is found to decrease from 0.254 to 0.225 ms with increasing temperature from 433 to 453 K. With increasing temperature, in the presence of oscillating field electron hops with faster rate between two localized ions and it takes lesser time (relaxation time) to come back to its original state.

Table 2: Resistance, capacitance and relaxation time values corresponds to bulk grain of $LiFePO_4$ at different temperatures

..

Temperature (K)	R_g (kΩ)	C_g (10^{-8} F)	τ_g (ms)
433	252	1.01	0.254
443	172	1.54	0.264
453	91	2.48	0.225

Semi-circles obtained for the $LiFePO_4$ can be represented by a RC electric circuit shown in Fig. 11, and analytically explained by Eqs. (4). Representation of sample through an electrical analog circuit is very helpful in representing the electrical features of the sample. In this circuit, a resistance represents a conductive path and a given resistor in a circuit might account for the bulk conductivity of the sample. Also the capacitances will be generally associated with space charge polarization regions. The equivalent circuit consists of a constant phase element (CPE), acting as a blocking double layer capacitance in series with the parallel combination of bulk resistance (R_g) and capacitor (C_g).

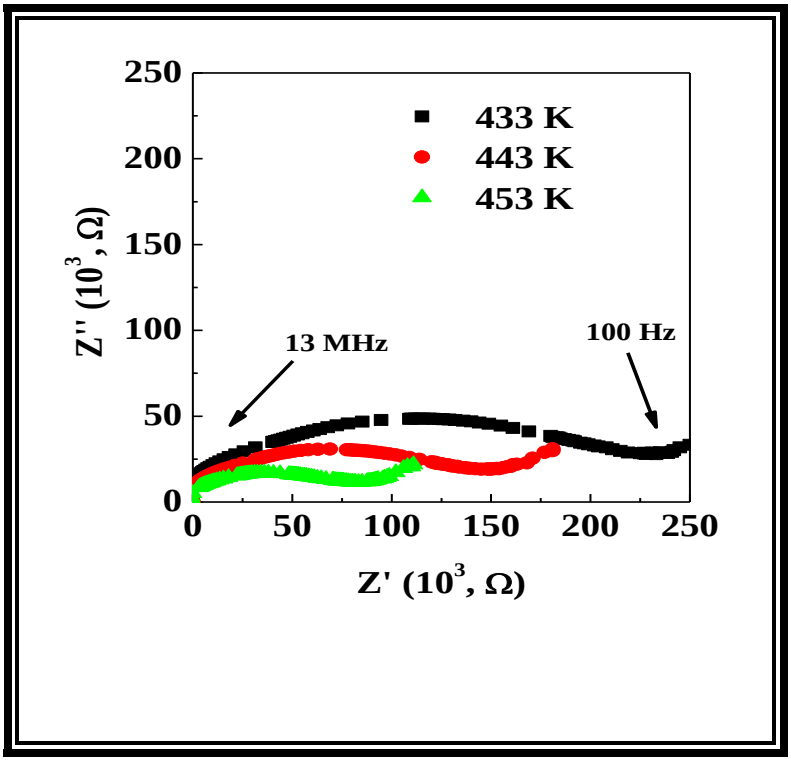

Figure 10: Cole-Cole plot of $LiFePO_4$ at different temperature

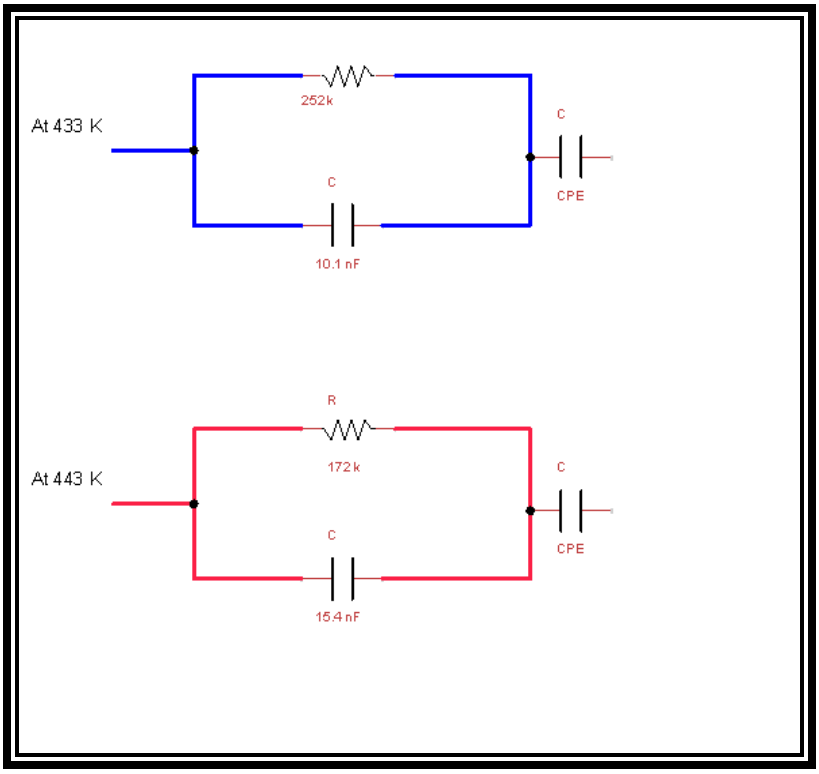

Figure 11: Equivalent circuits of $LiFePO_4$ at different temperatures

4.3 Electrical (DC) Conductivity

Temperature dependent dc conductivity of $LiFePO_4$ is shown in Fig. 12. The lnσ *vs* 1000/T plots (Fig. 12) indicate a slope, which is characteristic of the electrical conduction through an activated process. Temperature dependent conductivity is due to both hopping of electrons and charge transport via excited states which can be expressed as[98,99]

$$\sigma = A_1 \exp\left(\frac{-E_1}{k_B T}\right) + A_2 \exp\left(\frac{-E_2}{k_B T}\right) + A_3 \exp\left(\frac{-E_3}{k_B T}\right) + \ldots \qquad (7)$$

where E_1 is the activation energy for intrinsic conduction and E_2, E_3,…are the activation energies needed for hopping conduction. A_1, A_2, A_3 are constants and k_B is the Boltzmann constant. Activation energy (E_a) calculated from the lnσ *vs* 1000/T plot is 0.44 eV. Maier *et.al*[100] have reported E_a=0.43 eV, which is mainly due to the electronic conductivity in $LiFePO_4$. In the present case, the E_a value (0.44 eV) confirms that the conduction process in $LiFePO_4$ is due to the electronic and not ionic conduction. The dc electrical conductivity and E_a values obtained in the present case are in close agreement with those calculated from the first principle calculations and experimental reported values that account for the electronic transport to a polaron or electron hopping process.[101-103,104,105] In addition, anti-site defect is reported in $LiFePO_4$ concerning Li^+ and Fe^{2+} interchanged between two nonequivalent octahedral sites.[105] Interchange of Li and Fe ions or a Li vacancy owing to the anti site disorder is responsible for the hopping process. From first principle calculation and experimental observation, Xu *et.al* [104] have reported that the conduction in updoped $LiFePO_4$ is n-type and the low conductivity value is due to the large electron effective mass and less overlap between the Fe 3d orbitals due to lager Fe-Fe distance.

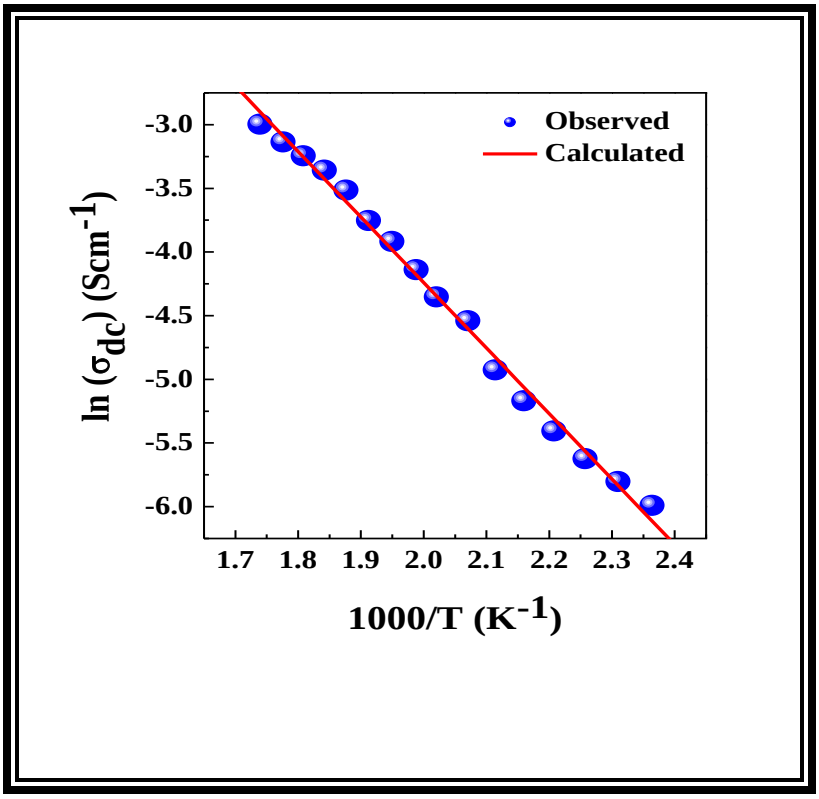

Figure 12: The relation between lnσdc and 1000/T of LiFePO4

4.4 Electrical (AC) Conductivity

The frequency dependence of real part of electrical conductivity (σ_{ac}) of $LiFePO_4$ at different temperatures is shown in Fig. 13. The total conductivity of $LiFePO_4$ can be expressed by the relationship[98,99]

$$\sigma_{tot} = \sigma_0(T) + \sigma(\omega, T) \qquad (8)$$

The first term σ_0 (T) of Eq. (7) represents the dc conductivity due to the band conduction, which is frequency independent. The second term of the equation is pure ac conductivity due to the electron hoping. Conductivity is seen to increase with increasing temperature as well as the frequency. At higher frequencies, the conductivity shows dispersion and as temperature increases the frequency at which the dispersion becomes prominent moves to higher frequency region. With increasing frequency and temperature, the hopping increases and correspondingly the conductivity increases. At 423 K while $\log(\sigma_{ac})$ ~ -6.08 Scm^{-1} at low frequencies (100 Hz), $\log(\sigma_{ac})$ increases to ~ -5.38 Scm^{-1} at higher frequencies (13 MHz). Observed conductivity values in the present case are well agreeing with that of reported values.[104,97]

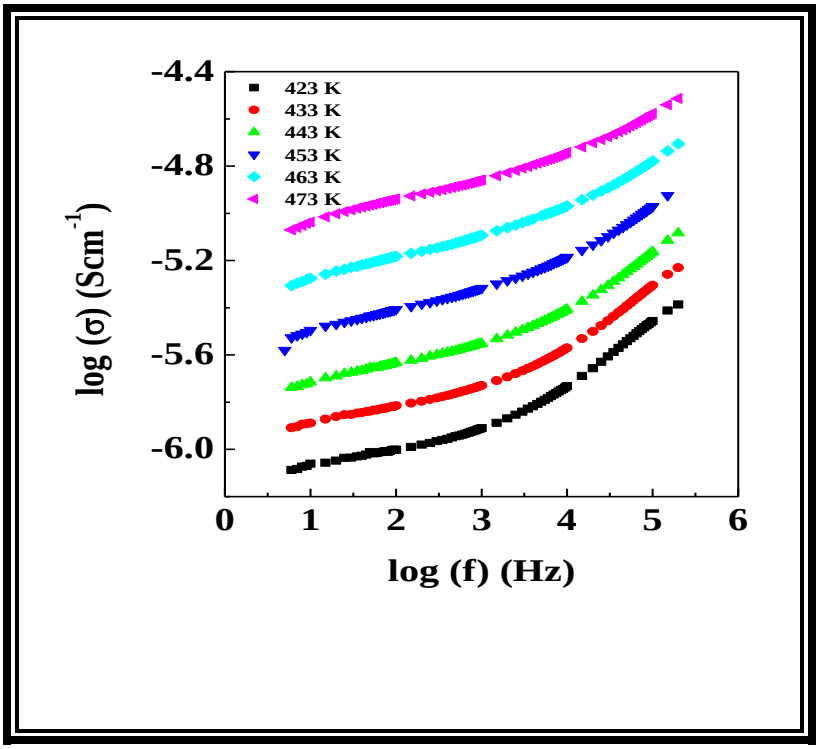

Figure 13: Frequency variation of AC conductivity of $LiFePO_4$

4.5 Dielectric Properties

Complex permittivity ($\varepsilon^*=\varepsilon' - i\varepsilon''$ where ε' and ε'' are the real and imaginary parts of the dielectric function) of $LiFePO_4$ has been calculated from the impedance data by using the following expression:[106]

$$\varepsilon^* = \frac{1}{j\omega C_0 Z^*} \qquad (9)$$

where Z^* is the complex impedance. $C_0 = \varepsilon_0 A/d$, is the capacitance of the empty cell. A and d are the area of the plate and thickness of the sample, respectively. The frequency variation of the real part of the dielectric constant (ε') at different temperatures for $LiFePO_4$ is presented in Fig. 14. It can be seen from the figure that the dielectric constant decreases with increasing frequency. The values of ε' (100 Hz) at 433 K and 473 K are 4.6 and 5.7 respectively. Increase in ε' with temperature can be explained as follows. The thermal energy, at sufficiently higher temperatures, liberates more localized dipoles and aligns to the field direction leading to an increase of the polarization as well as ε'.

The dispersion of ε' with frequency can be explained based on the contributions from various sources of polarizations. The larger value of ε at lower frequencies, perhaps, could be due to all the contributions (i.e, atomic, electronic, ionic, interfacial and grain-boundaries).[94-96] The decrease (and disappearance finally) in ionic and orientation polarizability with increasing frequency may be responsible for the decrease in ε' at higher frequencies.[102] Since more than one ion (O^{2-}, Li^+ and Fe^{3+} ions) contribute to the relaxation process, the data were fit to the modified Debye's function that considers the possibility of more than one ion, contributing to the relaxation. The observed dispersion of the dielectric constant can be modeled using the equation:[107]

$$\varepsilon' - \varepsilon_\infty = \frac{(\varepsilon_0 - \varepsilon_\infty)}{[1+(\omega\tau)^{2(1-\alpha)}]} \qquad (10)$$

where ε′ is the real part of the dielectric constant, ε_∞ is the dielectric constant at 13 MHz, τ is the mean relaxation time and α is the spreading factor of the actual relaxation times about the mean value. The fitting of the experimental data (at 433 K) to this model yield τ = 0.259 ms for $LiFePO_4$. It should be noted that this value is in agreement with the relaxation time value obtained from the Cole-Cole plot.

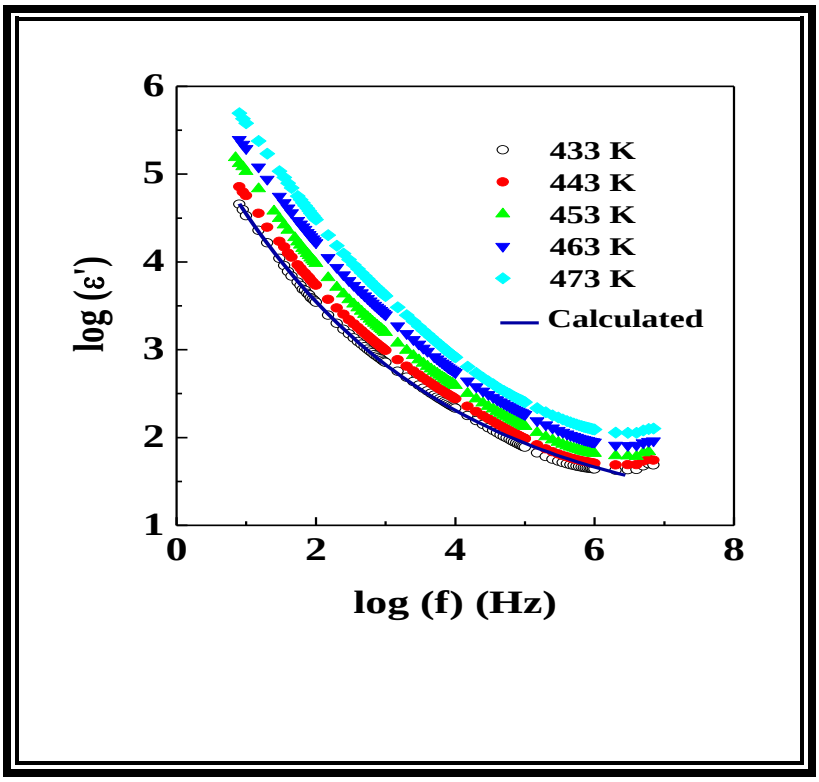

Figure14: Frequency variation of real part of the dielectric constant of LiFePO4 at different temperatures

Figure 15 shows the logarithmic variation of imaginary part of permittivity (ε′′) as a function of frequency at various temperatures. Conduction loss can be related to dc conductivity σ_{dc} by the following equation: [106]

$$\varepsilon'' = \frac{\sigma_{dc}}{\omega \varepsilon_0} \qquad (11)$$

ε'' is found to be decreases with increasing frequency. As temperature increases, the conductivity σ_{dc} increases and hence ε′′ also increases. There is no resonance peak observed for $LiFePO_4$ at various temperatures. Resonance peak takes place when jumping frequency of the localized charge carriers becomes approximately equal to that of the applied AC field.[95] Dielectric losses arise if the polarization lags behind the applied alternating field.

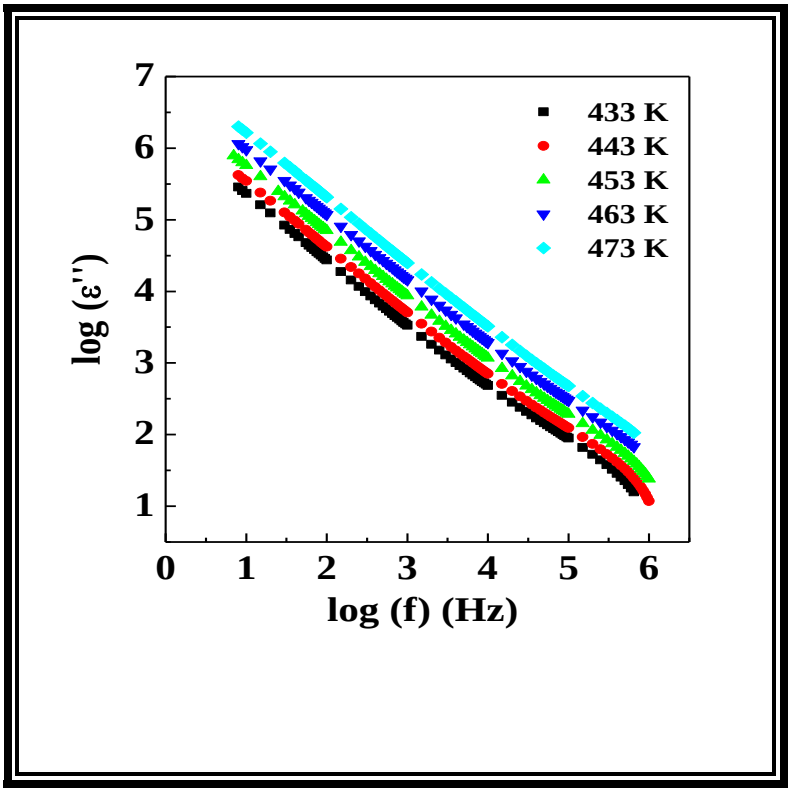

Figure 15: Frequency variation of imaginary part of the dielectric constant of LiFePO4 at different temperatures

CHAPTER 5: CONCLUSIONS AND FUTURE DIRECTIONS

Phase pure, microcrystalline $LiFePO_4$ was synthesized. Temperature and frequency dependent ac and dc electrical conductivity studies of $LiFePO_4$ indicate that the transport properties arise predominantly due to the electronic conduction. Frequency variation of the dielectric constant (ε′), Real (Z′) and imaginary part (Z′′) of impedance shows the dispersion and the existence of relaxation processes and their distribution in $LiFePO_4$. Temperature variation of dc electrical conductivity (σ_{dc}) (273-573 K) follows the Arrhenius relationship. Activation energy (E_a) calculated from the $\ln\sigma_{dc}$ *vs* 1000/T plot is found to be 0.44 eV, indicates the electronic conduction is predominant in $LiFePO_4$. A modeling or computer simulations of the interfacial phenomena and the associated electrical properties could provide a more detailed account of electrical properties of $LiFePO_4$ and related materials. This aspect opens the scope for future work.

REFERENCES

[1] Silberberg, M. 2006. Chemistry: The Molecular Nature of Matter and Change, 4th Ed. New York (NY): McGraw-Hill Education. p 935.

[2] K. Sekai, H. Azuma, A. Omaru et al., Lithium-ion rechargeable cells with $LiCoO_2$ and carbon electrodes. J. Power Sour.**43**,241-244(1993)

[3] S.L. Goodale, Chronology of Iron and Stell (Penton Publishing Co, Cleveland,1931)

[4] "LiFePO4: A Novel Cathode Material for Rechargeable Batteries", A.K. Padhi, K.S. Nanjundaswamy, J.B.Goodenough, Electrochemical Society Meeting Abstracts, 96-1, May, 1996, pp 73,

[5] "Next Generation Battery Technology Makes Hybrid and Electric Vehicles a Reality"(html). http://www.lithiumtech.com/pr51407.htm.lithiumtech.com

[6] D.P. Abraham, M.M. Furczon, S.-H. Kang, D.W. Dees, A.N. Jansen, Effect of electrolyte composition on initial cycling and impedance characteristics of lithium-ion cells, J. Power Sources 180 (2008) 612–620

[7] "Bigger, Cheaper, Safer Batteries: New material charges up lithium-ion battery work" (html).http://www.sciencenews.org/articles/20020928/fob4.asp. sciencenews.org

[8] page4- The trouble with lithium (http://www.meridian-int-res.com/Projects?Lithium_Microscope.pdf)

[9] Guo, Y.; Hu, J.; Wan, L. Nanostructured Materials for Electrochemical Energy Conversion and Storage Devices. Adv Mater 2008, 20, 2878-2887

[10]page4- The trouble with lithium (http://www.meridian-int-res.com/Projects?Lithium_Microscope.pdf)

[11]] Guo, Y.; Hu, J.; Wan, L. Nanostructured Materials for Electrochemical Energy Conversion and Storage Devices. Adv Mater 2008, 20, 2878-2887

[12] A123Systems (http://www.rc-netbutik.dk/getdoc.asp?id=100&md5hash=9810C237586CF6B4325753101E37DAE1) "...Current test projecting excellent calendar life: 17% impedance growth and 23% capacity loss in 15 [fifteen!] years at 100% SOC, 60 deg. C..."

[13] D. Guyomard, Advanced cathode materials for lithium batteries, in: Energy Storage Systems for Electronics, in: T. Osaka, M. Datta (Eds.), New Trends in Electrochemical Technology, vol. 1, Gordon and Breach, Amsterdam, 2000, pp. 253–350.

[14] M.S. Whittingham, Lithium batteries and cathode materials, Chem. Rev. 104 (2004) 4271–4301.

[15] A.K. Padhi, K.S. Nanjundaswamy, J. Goodenough, Phospho-olivines and positive-electrode materials for rechargeable lithium batteries, J. Electrochem. Soc. 144 (4) (1997) 1188–1194.

[16] A.K. Padhi, K.S. Nanjundaswamy, C. Masquelier, S. Okada, J. Goodenough, Effect of structure on the Fe^{3+}/Fe^{2+} redox couple in iron phosphates, J. Electrochem.Soc. 144 (5) (1997) 1609–1613.

[17] P. Axmann, C. Stinner, M. Wohlfahrt-Mehrens, A. Mauger, F. Gendron, C.M. Julien, Nonstoichiometric $LiFePO_4$: defects and related properties, Chem. Mater. 21 (8) (2009) 1636–1644.

[18] J. Chen, M.J. Vacchio, S. Wang, N. Chernova, P.Y. Zavalij, M.S. Whittingham, The hydrothermal synthesis and characterization of olivines and related compounds for electrochemical applications, Solid State Ionics 178 (2008) 1676–1693.

[19] J. Maier, R. Amin, Defect chemistry of $LiFePO_4$, J. Electrochem. Soc. 155 (4) (2008) A339–A344.

[20] G. Kobayashi, S.I. Nishimura, M.-S. Park, R. Kanno, M. Yashima, T. Ida, A. Yamada, Isolation of solid solution phases in size-controlled Li_xFePO_4 at room temperature, Adv. Funct. Mater. 19 (2009) 395–403.

[21] M. Maccario, L. Croguennec, B. Desbat, M. Couzi, F. Le Cras, L. Servant, Raman and FTIR spectroscopy investigations of carbon-coated Li_xFePO_4 materials, J. Electrochem. Soc. 155 (12) (2008) A879–A886.

[22] U.S. Kasavajjula, C. Wang, P.E. Arce, Discharge model for LiFePO4 accounting for the solid solution range, J. Electrochem. Soc. 155 (11) (2008) A866–A874.

[23] R. Dedryvere, M. Maccario, L. Croguennec, F. Le Cras, C. Delmas, D. Gonbeau, X-Ray photoelectron spectroscopy investigations of carbon-coated Li_xFePO_4 materials, Chem. Mater. 20 (22) (2008) 7164–7170.

[24] J.L. Allen, T.R. Jow, J. Wolfenstine, Analysis of the $FePO_4$ to $LiFePO_4$ phase transition, J. Solid State Electrochem. 12 (2008) 1031–1033.

[25] N. Meethong, Y.-H. Kao, M. Tang, H.-Y. Huang, W.C. Carter, Y.-M. Chiang, Electrochemically induced phase transformation in nanoscale olivines $Li_{1-x}MPO_4$ (M= Fe, Mn), Chem. Mater. 20 (19) (2008) 6189–6198.

[26] W. Sigle, R. Amin, K. Weichert, P.A. van Aken, J. Maier, Delithiation study of $LiFePO_4$ crystals using electron energy-loss spectroscopy, Electrochem. Solid- State Lett. 12 (8) (2009) A151–A154.

[27] S.G. Stewart, V. Srinivasan, J. Newman, Modeling the performance of lithiumion batteries and capacitors during hybrid-electric-vehicle operation, J. Electrochem. Soc. 155 (9) (2008) A664–A671.

[28] B. Ellis, L.K. Perry, D.H. Ryan, L.F. Nazar, Small polaron hopping in Li_xFePO_4 solid solutions: coupled lithium-ion and electron mobility, J. Am. Chem. Soc.128 (2006) 11416–11422

[29] M.S. Whittingham, Lithium batteries and cathode materials, Chem. Rev. 104 (2004) 4271–4301.

[30] R. Amin, J. Maier, Effect of annealing on transport properties of $LiFePO_4$: towards a defect chemical model, Solid State Ionics 178 (2008) 1831–1836.

[31] M.S. Whittingham, Inorganic nanomaterials for batteries, Dalton Trans. 40 (2008) 5424–5431.

[32] Chung SY,Bloking JT, Chiang YM(2002) Nat Mater 1:123 doi:10.1038/nmat732

[33] (McKinnon WR, Hearing RR(1987) Modern aspect in electrochemistry. Plenum, New York

[34] S.M. Islam, D.J. Driscoll, C.A.J. Fisher, P.R. Slater, Chem. Mater. 17 (2005) 5085.

[35] D. Morgan, A.V.D. Ven, G. Ceder, Electrochem. Solid State Lett. 7 (2004) A30.

[36] C.V. Ramana, A. Mauger, F. Gendron, C.M. Julien , K. Zaghib . Study of the Li-insertion/extraction process in $LiFePO_4/FePO_4$,Journal of Power Sources 187 (2009) 555–564.

[37] M.S. Whittingham, Y. Song, S. Lutta, P.Y. Zavalij, N.A. ChernovaJ. Mater. Chem. 15 (2005), p. 3362)

[38] Y. Lin, M.X. Gao, D. Zhu, Y.F. Liu, H.G. Pan, Effects of carbon coating and iron phosphides on the electrochemical properties of $LiFePO_4$/C, J. Power Sources 184 (2008) 444–448.

[39] H. Nakano, K. Dokko, S. Koizumi, H. Tannaa, K. Kanamura, Hydrothermal synthesis of carbon-coated $LiFePO_4$ and its application to lithium polymer battery, J. Electrochem. Soc. 155 (12) (2008) A909–A914.

[40] P. He, X. Zhang, Y.-G. Wang, L. Cheng, Y.-Y. Xia, Lithium-ion intercalation behavior of LiFePO4 in aqueous and nonaqueous electrolyte solutions, J. Electrochem. Soc. 155 (2) (2008) A144–A150.

[41] X. Zhi, G. Liang, L. Wang, X. Ou, J. Zhang, J. Cui, The cycling performance of LiFePO4/C cathode materials, J. Power Sources 189 (2009) 779–782.

[42] K. Wang, R. Cai, T. Yuan, X. Yu, R. Ran, Z. Shao, Process investigation, electrochemical characterization, optimization of $LiFePO_4$/C composite from mechanical activation using sucrose as carbon source, Electrochim. Acta 54 (2009) 2861–2868.

[43] S. Lim, C.S. Yoon, J. Cho, Synthesis of nanowire and hollow $LiFePO_4$ cathodes for high-performance lithium batteries, Chem. Mater. 20 (14) (2008) 4560–4564.

[44] J.-M. Chen, C.-H. Hsu, Y.-R. Lin, M.-H. Hsiao, G.T.-K. Fey, High-power $LiFePO_4$ cathode materials with a continuous nano carbon network for lithium-ion batteries, J. Power Sources 184 (2008) 498–502.

[45] B. Zhao, Y. Jiang, H. Zhang, H. Tao, M. Zhong, Z. Jiao, Morphology and electrical properties of carbon coated $LiFePO_4$ cathode materials, J. Power Sources 189 (2009) 462–466.

[46] Y.Z. Dong, Y.M. Zhao, Y.H. Chen, Z.F. He, Q. Kuang, Optimized carbon-coated $LiFePO_4$ cathode material for lithium-ion batteries, Mater. Chem. Phys. 115 (2009) 245–250.

[47] Z.-R. Chang, H.-J. Lv, H.-W. Tang, H.-J. Li, X.-Z. Yuan, H. Wang, Synthesis and characterization of high-density $LiFePO_4$/composites as cathode materials for lithium-ion batteries, Electrochim. Acta 54 (2009) 4595–4599.

[48] Y. Yang, X.-Z. Liao, Z.-F. Ma, B.-F. Wang, L. He, Y.-S. He, Superior high-rate cycling performance of $LiFePO_4$/C-PPy composite at 55 ◦C, Electrochem. Commun.11 (2009) 1277–1280.

[49] Y. Zhao, D. Xia, Y. Li, C. Yu, Investigation of high-rate spherical $LiCoO_2$ with mesoporous structure via self-assembly in microemulsion, Electrochem. Solid-State Lett. 11 (3) (2008) A30–A33.

[50] M. Okubo, E. Hosono, T. Kudo, H.S. Zhou, I. Honma, Size effect on electrochemical property of nanocrystalline $LiCoO_2$ synthesized from rapid thermal annealing method, Solid State Ionics 180 (2008) 612–615.

[51] W. Kim, J.-J. Cho, Y. Kang, D.-W. Kim, Study on cycling performances of lithium-ion polymer cells assembled by in situ chemical cross-linking with star-shaped siloxane acrylate, J. Power Sources 178 (2008) 837–841.

[52] E.-G. Shim, T.-H. Nam, J.-G. Kim, H.-S. Kim, S.-I. Moon, Diphenyloctyl phosphate as a flame-retardant additive in electrolyte for Li-ion batteries, J. Power Sources 175 (2008) 533–539.

[53] J.-T. Lee, Y.-J. Chu, X.-W. Peng, F.-M. Wang, C.-R. Yang, C.-C. Li, A novel and efficient water-based composite binder for $LiCoO_2$ cathodes in lithium-ion batteries, J. Power Sources 173 (2007) 985–989.

[54] P. Albertus, J. Christensen, J. Newman, Experiments on and modeling of positive electrodes with multiple active materials for lithium-ion batteries, J. Electrochem. Soc. 156 (7) (2009) A606–A618.

[55] G. Li, Z. Yang, W. Yang, Effect of $FePO_4$ coating on electrochemical and safety performance of LiCoO2 as cathode material for Li-ion batteries, J. Power Sources 183 (2008) 741–748.

[56] J.F. Whitacre, K. Zaghib, W.C. West, B.V. Ratnakumar, Dual active material composite cathode structures for Li-ion batteries, J. Power Sources 177 (2008) 528–536.

[57] S.-B. Kim, K.J. Lee, W.J. Choi, W.-S. Kim, I.C. Jang, H.H. Lim, Y.S. Lee, Preparation and cycle performance at high temperature for $Li(Ni_{0.5}Co_{0.2}Mn_{0.3}])_2$ coated with $LiFePO_4$, J. Solid State Electrochem., in press, doi:10.1007/s10008-009-0873-7.

[58] S.-H. Kang, M.M. Thackeray, Enhancing the rate capability of high capacity $xLi_2MnO_3{\cdot}(1-x)LiMO_2$ (M=Mn, Ni, Co) electrodes by Li–Ni–PO_4 treatment, Electrochem. Commun. 11 (2009) 748–751.

[59] Z. Su, S.H. Ye, T.Y. Yan, X.P. Gao, P.W. Shen, Synthesis and electrochemical properties of nanosized $LixMnO_2$ as cathode materials for lithium batteries, J. Electrochem. Soc. 155 (11) (2008) A839–A844.

[60] Z.-R. Chang, H.-J. Lv, H.-W. Tang, H.-J. Li, X.-Z. Yuan, H. Wang, Synthesis and characterization of high-density $LiFePO_4$/composites as cathode materials for lithium-ion batteries, Electrochim. Acta 54 (2009) 4595–4599.

[61] C.-Z. Lu, G.T.-K. Fey, H.-M. Kao, Study of $LiFePO_4$ cathode materials coated with high surface area carbon, J. Power Sources 189 (2009) 155–162.

[62] J.L. Jones, J.-T. Hung, Y.S. Meng, Intermittent X-ray diffraction study of kinetics of delithiation in nano-scale $LiFePO_4$, J. Power Sources 189 (2009) 702– 705.

[63] H. Joachin, T.D. Kaun, K. Zaghib, J. Prakash, Electrochemical and thermal studies of carbon-coated $LiFePO_4$ cathode, J. Electrochem. Soc. 156 (6) (2009) A401–A406.

[64] Y.-D. Cho, G.T.-K. Fey, H.-M. Kao, The effect of carbon coating thickness on the capacity of $LiFePO_4$/C composite cathodes, J. Power Sources 189 (2009) 256–262.

[65] H.H. Li, J. Jin, J.P. Wei, Z. Zhou, J. Yan, Fast synthesis of core-shell $LiCoPO_4$/C nanocomposite via microwave heating and its electrochemical Li intercalation performances, Electrochem. Commun. 11 (2009) 95–98.

[66] M. Maccario, L. Croguennec, B. Desbat, M. Couzi, F. Le Cras, L. Servant, Raman and FTIR spectroscopy investigations of carbon-coated Li_xFePO_4 materials, J Electrochem. Soc. 155 (12) (2008) A879–A886.

[67] M.M. Doeff, J.D. Wilcox, R. Yu, A. Aumentado, M. Marcinek, R. Kostecki, Impact of carbon structure and morphology on the electrochemical performance of $LiFePO_4$/C composites, J. Solid State Electrochem. 12 (2008) 995–1001.

[68] Y.-H. Nien, J.R. Carey, J.-S. Chen, Physical and electrochemical properties of $LiFePO_4$/C composite cathode prepared from various polymer-containing precursors, J. Power Sources 193 (2009) 822–827.

[69] X. Yan, G. Yang, J. Liu, Y. Ge, H. Xie, X. Pan, R. Wang,Aneffective and simpleway to synthesize $LiFePO_4$/C composite, Electrochim. Acta 54 (2009) 5770–5774.

[70] J.-M. Chen, C.-H. Hsu, Y.-R. Lin, M.-H. Hsiao, G.T.-K. Fey, High-power $LiFePO_4$ cathode materials with a continuous nano carbon network for lithium-ion batteries, J. Power Sources 184 (2008) 498–502.

[71] W. Guoping, Z. Qingtang, Y. Zuolong, Q. MeiZheng, The effect of different kinds of nano-carbon conductive additives in lithium ion batteries on the resistance and electrochemical behavior of the $LiCoO_2$ composite cathodes, Solid State Ionics 179 (2008) 263–268.

[72] B. Jin, E.M. Jin, K.-H. Park, H.-B. Gu, Electrochemical properties of $LiFePO_4$- multiwalled carbon nanotubes composite cathode materials for lithium polymer battery, Electrochem. Commun. 10 (2008) 1537–1540.

[73] B. Jin, H.-B. Gu, W. Zhang, K.-H. Park, G. Sun, Effect of different carbon conductive additives on electrochemical properties of $LiFePO_4$-C/Li batteries, J. Solid State Electrochem. 12 (2008) 1549–1554.

[74] M.S. Bhuvaneswari, N.N. Bramnik, D. Ensling, H. Ehrenberg, W. Jaegermann, Synthesis and characterization of carbon nano fiber/$LiFePO_4$ composites for Li-ion batteries, J. Power Sources 180 (2008) 553–560.

[75] Y. Liu, X. Li, H. Guo, Z. Wang, W. Peng, Y. Yang, R. Liang, Effect of carbon nanotube on the electrochemical performance of C-$LiFePO_4$/graphite battery,J. Power Sources 184 (2008) 522 -526.

[76] D. Rangappa, M. Ichihara, T. Kudo, I. Honma, Surface modified $LiFePO_4$/C nanocrystals synthesis by organic molecules assisted supercritical water process molecules assisted supercritical water process, J. Power Sources 194 (2009) 1036–1042.

[77] G.T.-K. Fey, C.-S. Chang and T.P. Kumar, Synthesis and surface treatment of $LiNi_{1/3}Co_{1/3}Mn_{1/3}O_2$ cathode materials for Li-ion batteries, J. Solid State Electrochem.,in press, doi:10.1007/s10008-008-0772-3.

[78] B. Jin, H.-B. Gu, K.-W. Kim, Effect of different conductive additives on charge/discharge properties of $LiCoPO_4$/Li batteries, J. Solid State Electrochem.12 (2008) 105–111.

[79] A. Yamada, S.C. Chung, K. Hinokuma, J. Electrochem. Soc. 148 (2001) A224.

[80] A. Yamada, S.C. Chung, J. Electrochem. Soc. 148 (2001) A96.

[81] S. Yang, Y. Song, P.Y. Zavalij, M.S. Whittingham, J. Electrochem. Commun. 4 (2002) 239.

[82] J.D. Wilcox, M.M. Doeff, M. Marcinek, R. Kostecki, J. Electrochem. Soc. 154 (2007) A389.

[83] I. Belharouak, C. Johnson, K. Amine, J. Electrochem. Commun. 7 (2005) 983.

[84] F. Croce, A.D. Epifanio, J. Hassoun, A. Deptula, T. Olezac, B. Scrosati, Electrochem. Solid-State Lett. 5 (2002) A47.

[85] M. Takahashi, S. Tobishima, K. Takei, Y. Sakurai, J. Power. Sources 97–98 (2001) 508.

[86] S.Y. Chung, J.T. Bloking, Y.-M. Chiang, Nat. Mater. 1 (2002) 123.

[87] Z. Chen, J.R. Dahn, J. Electrochem. Soc. 149 (2002) A1184.

[88] C. Wurm, M. Moorcette, S.Gwizdala, and C. Masquelier, Word Pat. WO 02/099913 A1 (2002).

[89] N. Ravet, Y. Chouinard, J.F.Magnan, S. Besner, M. Gauthier, M. Armand, J. Power. Sources 97–99 (2001) 503.

[90] H. Huang, S.C. Yin, L.F. Nazar, Electrochem. Solid-State Lett. 4 (2001) A170.

[91] J.M. Chen, C.H. Hsu, Y.R Lin, M.H.Hsiao, G.T.K.Fey, J. Power.Source 498–502(2008)184.

[92]. A.C. Larson and R.B. Von Dreele, General Structure Analysis System (GSAS), Los Alamos National Laboratory Report LAUR 86-748 (2004)

[93]. M. Bini, M. C. Mozzati, P. Galinetto, D. Capsoni, S. Ferrai, M.S. Grandi, V. Massarotti, J. Solid State Chem, 182 (2009) 1972

[94]. J. Smith, H. P. J. Wijn, *Ferrites,* (1965), Philips Technical Library, Eindhoven- Holland.

[95]. K. Kamala Bharathi, G. Markandeyulu, C.V. Ramana, J. Electrochem. Soc. 158 (2011) G71.

[96]. J. T. S. Irvine, D. C. Sinclair, A. R. West, Adv. Mater. 2 (2004) 132.

[97]. R. Amin, J. Maier, Solid State Ionics 178 (2008) 1831.

[98]. Anderson, Dielectrics, (1964) (Spottiswoode, Ballantyne & Co Ltd, London)

[99]. R. S. Vemuri, K. Kamala Bharathi, S. K. Gullapalli, C. V. Ramana, ACS Appl. Mater. Interfaces 2 (2010) 2623.

[100]. J. Maier, R. Amin, J. Electrochem. Soc.155 (2008) A339.

[101]. T. Maxisch, F. Zhou, G. Ceder, Phys. Rev. B 73 (2006) 104301.

[102]. S. Shi, C. Ouyang, Z. Xiong, L. Liu, Z. Wang, H. Li, D.S. Wang, L. Chen, X. Huang, Phys. Rev. B 71 (2005) 144404.

[103]. S. Shi, L. Liu, C. Ouyang, D.S. Wang, Z. Wang, L. Chen, X. Huang, Phys. Rev. B 68 (2003) 195108.

[104]. Y. N. Xu, S. Y. Chung, J. T. Bloking, Y. M. Chiang, W. Y. Ching, Electrochem. Solid State Lett. 7 (2004) A131.

[105]. K. Zaghib, A. Mauger,,J. B. Goodenough, F. Gendron, C. M. Julien, Chem. Mater. 19 (2007) 3740.

[106]. Laxmi Narayana Patro, K. Hariharan, Mater. Chem. Phys. 116 (2009) 81.

[107]. K. Kamala Bharathi, G. Markandeyulu, C. V. Ramana, *Electrochem. Solid-State Lett.*, 13 (2010) G98.

VITA

Sukhdeep Amarjeet Labana was born on June 03 of 1986 in Tanda Urmur Punjab (INDIA). She started her career at the Nagpur University India in fall 2006. By the Summer of 2010 Sukhdeep graduated with a bachelor's degree in Power Electrical Engineering. As undergraduate student she served as project leader in leading other volunteers in completing assignments and team goals in her project "Energy Audit of S.R.K.N.E.C." During the Spring of 2011 she joined University of Texas at El Paso (UTEP) to pursue Masters in Electrical and Computer Engineering. During the Course work of her studies she joined Public Professional Program at UTEP and held Summer Classes for the students. She was also acknowledged by 'The Assayer of student prospector' as the Mentor to help students deal with the financle burdens of college. As a volunteer experience she provided administrative support in preparing paper presentation, organizing seminars, coordinating events, and supervising sports competition.

Permanent Address: 213 Argonaut Drive Apt#21

El Paso, Texas, 79912

This thesis was typed by Sukhdeep Labana.